

Suppressing electromagnetic local density of states via slow light in lossy quasi-one-dimensional gratings

Benjamin Strekha ^{1,*}, Pengning Chao ^{2,*}, Rodrick Kuate Defo ¹, Sean Molesky ³, and Alejandro W. Rodriguez¹

¹*Department of Electrical and Computer Engineering, Princeton University, Princeton, New Jersey 08544, USA*

²*Department of Mathematics, Massachusetts Institute of Technology, Cambridge, Massachusetts 02139, USA*

³*Department of Engineering Physics, Polytechnique Montréal, Montréal, Québec H3T 1J4, Canada*



(Received 27 September 2023; accepted 21 March 2024; published 11 April 2024)

We propose a spectral-averaging procedure that enables the computation of bandwidth-integrated local density of states (LDOS) from a single scattering calculation, and exploit it to investigate the minimum extinction achievable from dipolar sources over nonzero bandwidths in structured media. Structure-agnostic extinction bounds are derived, providing analytical insights into scaling laws and fundamental design tradeoffs with implications to bandwidth and material selection. We find that perfect LDOS suppression over a nonzero bandwidth $\Delta\omega$ is impossible. Inspired by limits which predict nontrivial $\sqrt{\Delta\omega}$ scaling in systems with material dissipation, we show that the pseudogap edge states of quasi-one-dimensional bullseye gratings can—by simultaneously minimizing material absorption and radiation—yield arbitrarily close to perfect LDOS suppression in the limit of vanishing bandwidth.

DOI: [10.1103/PhysRevA.109.L041501](https://doi.org/10.1103/PhysRevA.109.L041501)

Introduction. The electromagnetic local density of states (LDOS) plays a central role in many optical phenomena, including spontaneous [1] and stimulated emission [2], radiating antennas, surface-enhanced Raman scattering [3,4], photovoltaics [5], radiative heat transfer [6], and frequency conversion [7]. Canonically, changing the electromagnetic environment of a quantum emitter alters its rate of spontaneous emission [8]. Furthermore, suppressing radiative processes can reduce losses in semiconductor lasers [9] and increase parametric nonlinearities [7].

In this Letter, we exploit quadratic optimization techniques to explore the minimum bandwidth-integrated LDOS possible in structured media. Calculations are vastly simplified by the fact that LDOS, proportional to the power extracted from a subwavelength emitter, is a causal linear-response function, allowing one to relate the bandwidth-integrated response to the evaluation of the integrand at a single, complex frequency (plus a non-negative electrostatic contribution); this in turn makes techniques for computing single-frequency bounds [10–13] applicable to finite-bandwidth objectives. Prior applications of such contour-deformation techniques employed a Lorentzian spectral window that leads to ultraviolet divergences in the vacuum response [11,13,14] and is therefore only appropriate for studying scattered power; it is unsuitable for quantifying Purcell enhancement and particularly LDOS suppression, which relies on sensitive cancellations between contributions from the radiating source and scatterer. To remedy this issue, we introduce an averaging function that behaves similar to a Lorentzian for small bandwidths, exhibiting a single pole in the upper half plane while decaying sufficiently fast so as to avoid such ultraviolet divergences.

Our bounds show that no structures can completely suppress LDOS for nonzero bandwidths. Intuitively, photonic crystals (PhCs), which support complete photonic band gaps and thus inhibit wave propagation at frequencies within the gap [15], are a natural guess for the optimal suppression of average LDOS. For lossless materials, PhCs and Bragg gratings are optimal geometries for any bandwidth but can only achieve perfect suppression in the limit of vanishing bandwidth (a single frequency), as they are unable to suppress radiation at frequencies outside the band gap. Surprisingly, we find that near-perfect suppression at a single frequency is also feasible in the presence of material loss. For a PhC in two dimensions (2D), a minimal index contrast and hence minimum feature size is needed to open a gap [16–18], which limits the degree to which absorption can be mitigated, leading to LDOS saturation. Quasi-1D structures, on the other hand, such as bullseye gratings supporting pseudogap “slow light” resonances with low-field concentrations in the dielectric medium, approach zero extinction power in the limit of vanishing material thicknesses by enabling the gap to close more slowly than absorption.

Formulation. Working in dimensionless units of $\epsilon_0 = \mu_0 = 1$, and considering only nonmagnetic materials, the partial LDOS at frequency ω and position \mathbf{r}' along the direction $\hat{\mathbf{e}}$ is directly proportional to the time-averaged power $\rho(\omega)$ emitted by a harmonic dipole source $\mathbf{J}(\mathbf{r}; \omega)e^{-i\omega t} = \delta(\mathbf{r} - \mathbf{r}')e^{-i\omega t}\hat{\mathbf{e}}$ [19,20],

$$\rho(\omega) \equiv -\frac{1}{2} \operatorname{Re} \int \mathbf{J}^*(\mathbf{r}; \omega) \cdot \mathbf{E}(\mathbf{r}; \omega) d\mathbf{r}, \quad (1)$$

where the electric field generated by the current \mathbf{J} satisfies Maxwell’s equations, $\nabla \times \nabla \times \mathbf{E}(\mathbf{r}) - \omega^2[1 + \chi(\mathbf{r})]\mathbf{E}(\mathbf{r}) = i\omega\mathbf{J}(\mathbf{r})$. We can decompose the total field into the field emitted by the source in vacuum and that emitted by the induced

*These authors contributed equally to this work.

polarization \mathbf{P} within the scatterer,

$$\begin{aligned} \mathbf{E}(\mathbf{r}) &= \mathbf{E}_{\text{vac}}(\mathbf{r}) + \mathbf{E}_{\text{sca}}(\mathbf{r}) \\ &= \frac{i}{\omega} \int \mathbb{G}_0(\mathbf{r}, \mathbf{r}') \cdot \mathbf{J}(\mathbf{r}') d\mathbf{r}' + \int \mathbb{G}_0(\mathbf{r}, \mathbf{r}') \cdot \mathbf{P}(\mathbf{r}') d\mathbf{r}', \end{aligned} \quad (2)$$

where $\mathbb{G}_0(\mathbf{r}, \mathbf{r}')$ is the vacuum dyadic Green's function, satisfying $\nabla \times \nabla \times \mathbb{G}_0 - \omega^2 \mathbb{G}_0 = \omega^2 \mathbb{I}$. This in turn leads to a decomposition of ρ into vacuum and scatterer contributions

$$\rho(\omega) = \rho_{\text{vac}}(\omega) + \rho_{\text{sca}}(\omega), \quad (3)$$

where ρ_{vac} and ρ_{sca} are defined by substituting \mathbf{E}_{vac} and \mathbf{E}_{sca} into Eq. (1), respectively. In particular,

$$\rho_{\text{sca}}(\omega) = -\frac{1}{2} \text{Im} \omega \int \mathbf{E}_{\text{vac}}(\mathbf{r}') \cdot \mathbf{P}(\mathbf{r}') d\mathbf{r}' \equiv \text{Im} s(\omega), \quad (4)$$

where we use the irrelevancy of the global phase of the source to set $\mathbf{J}^*(\mathbf{r}; \omega) = \mathbf{J}(\mathbf{r}; \omega)$, and reciprocity $\mathbb{G}_0 = \mathbb{G}_0^T$.

Since real sources emit light over a nonzero bandwidth, a key figure of merit is the bandwidth average of $\rho(\omega)$. Prior works focused on LDOS enhancement have investigated an averaging of the form $\int_{-\infty}^{\infty} \rho(\omega) L(\omega) d\omega$, where

$$L(\omega) \equiv \frac{\Delta\omega/\pi}{(\omega - \omega_0)^2 + \Delta\omega^2} \quad (5)$$

is a Lorentzian window function centered at ω_0 with bandwidth $\Delta\omega$ [11,13,14]. $L(\omega)$ not only captures the spectral line shape of many practical sources [14,21] but also offers a great computational advantage: Complex contour integration simplifies the frequency integral to a single evaluation $\rho(\tilde{\omega})$ at the complex pole $\tilde{\omega}$ of $L(\omega)$ in the upper half plane, plus an electrostatic contribution. However, there is one conceptual challenge: In the ultraviolet limit $\omega \rightarrow \infty$, $\rho_{\text{vac}}(\omega)$ grows too quickly ($\propto |\omega|$ in 2D and $\propto \omega^2$ in 3D) causing the Lorentzian spectral average to diverge [14]. When investigating LDOS maximization, ρ_{vac} and ρ_{sca} have the same sign, and this vacuum divergence can be ignored as a constant background (precluding, however, determination of the Purcell factor and related LDOS enhancement figures of merit [8,19]). Minimizing extinction, however, requires engineering ρ_{sca} to cancel ρ_{vac} , making this procedure prohibitive.

To remedy this issue, we define an alternate bandwidth average over the positive frequencies as follows,

$$\langle Q \rangle \equiv \lim_{\epsilon \rightarrow 0^+} \int_{\epsilon}^{\infty} Q(\omega) W(\omega) d\omega \quad (6)$$

$$= \lim_{\epsilon \rightarrow 0^+} \int_{\epsilon}^{\infty} Q(\omega) \left[\frac{L(\omega) - L(-\omega)}{\omega \mathcal{N}} \right] d\omega, \quad (7)$$

with the normalization factor $\mathcal{N} \equiv \frac{\omega_0}{\omega_0^2 + \Delta\omega^2}$ chosen so that $\int_0^{\infty} W(\omega) d\omega = 1$, with $W(\omega)$ non-negative and finite for $\omega \in (0, \infty)$. Figure 1 shows this window function which in most practical settings with $\Delta\omega \ll \omega_0$ resembles a Lorentzian distribution peaked around ω_0 ; for large bandwidths $\Delta\omega \gtrsim \omega_0$ the spectrum becomes increasingly asymmetric about ω_0 and gives greater weight to quasistatic contributions. Since $W(\omega) \sim \omega^{-4}$ as $\omega \rightarrow \infty$, $\langle \rho_{\text{vac}} \rangle$ is a convergent quantity that can be evaluated directly.

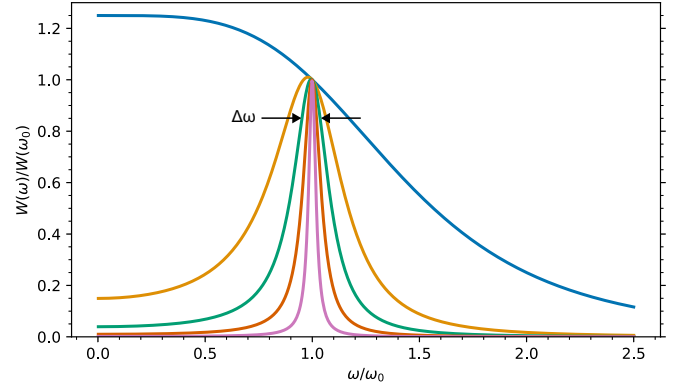


FIG. 1. Spectral window function $W(\omega)$ used in calculating average LDOS around a “center” frequency ω_0 , Eq. (6), for various values of the bandwidth parameter $\Delta\omega = \{1, \frac{1}{5}, \frac{1}{10}, \frac{1}{20}, \frac{1}{50}\}\omega_0$ (top to bottom). For ease of visualization, $W(\omega)$ is normalized by $W(\omega_0)$.

Since the Fourier components of real fields at negative frequencies are conjugates of the counterparts at positive frequencies [22], $\rho_{\text{sca}}(\omega) = \rho_{\text{sca}}(-\omega)$ and Eq. (7) can be unfolded into a principal value integral over all positive and negative frequencies:

$$\langle \rho_{\text{sca}} \rangle = \text{Im P.V.} \int_{-\infty}^{\infty} \frac{L(\omega)}{\omega \mathcal{N}} s(\omega) d\omega. \quad (8)$$

This can be evaluated using contour integration, yielding

$$\langle \rho_{\text{sca}} \rangle = \text{Im} \left[\frac{s(\tilde{\omega})}{\tilde{\omega} \mathcal{N}} \right] + \frac{2\omega_0 \Delta\omega}{|\tilde{\omega}|^4 \mathcal{N}} \alpha, \quad (9)$$

where the first term is from the residue at $\tilde{\omega} \equiv \omega_0 + i\Delta\omega$, the pole of $L(\omega)$ in the upper half plane; the second term is a non-negative electrostatic contribution due to the singularity at $\omega = 0$: here, $\alpha = \frac{1}{2} \text{Re} \mathbf{p}_0 \cdot \mathbf{E}_0$, where \mathbf{p}_0 is a unit amplitude electrostatic dipole and \mathbf{E}_0 the scattered field it generates, previously seen in Refs. [11,13] but with a different prefactor due to our use of $W(\omega)$ instead of $L(\omega)$.

The average of allowed modifications in the emission rate around the “center” frequency ω_0 (e.g., the spontaneous emission of an atom of corresponding transition energy) is constrained in all cases by this simple “weighted-sum rule.” In the limit of zero bandwidth, only the first term in Eq. (9) is in general nonzero, which represents single-frequency LDOS: $\langle \rho \rangle = \rho_{\text{vac}}(\omega_0) + \rho_{\text{sca}}(\omega_0)$. As the bandwidth goes to infinity, $\text{Im} \left[\frac{s(\tilde{\omega})}{\tilde{\omega} \mathcal{N}} \right]$ decays rapidly and the second term can be shown (under proper normalization of the window function) to yield an all-frequency sum rule $\int_0^{\infty} \rho_{\text{sca}}(\omega) d\omega = \pi \alpha / 2$ [11].

Since we are seeking lower bounds on $\langle \rho \rangle$, the non-negative electrostatic term α can be relaxed to zero; for transverse magnetic (TM) sources, it is exactly zero [23,24]. We then adapt the method laid out in Ref. [13] for computing upper bounds on LDOS maximization to instead obtain lower bounds on the remaining term $\text{Im} \left[\frac{s(\tilde{\omega})}{\tilde{\omega} \mathcal{N}} \right]$: Given a prespecified design region V and an isotropic material susceptibility $\chi(\tilde{\omega})$, the bounds enforce conservation of power (optical theorem [19,25]) constraints and apply to any structure that fits within V .

Note that the averaging procedure requires $\chi(\tilde{\omega})$ to be evaluated at a complex frequency, with causality and loss

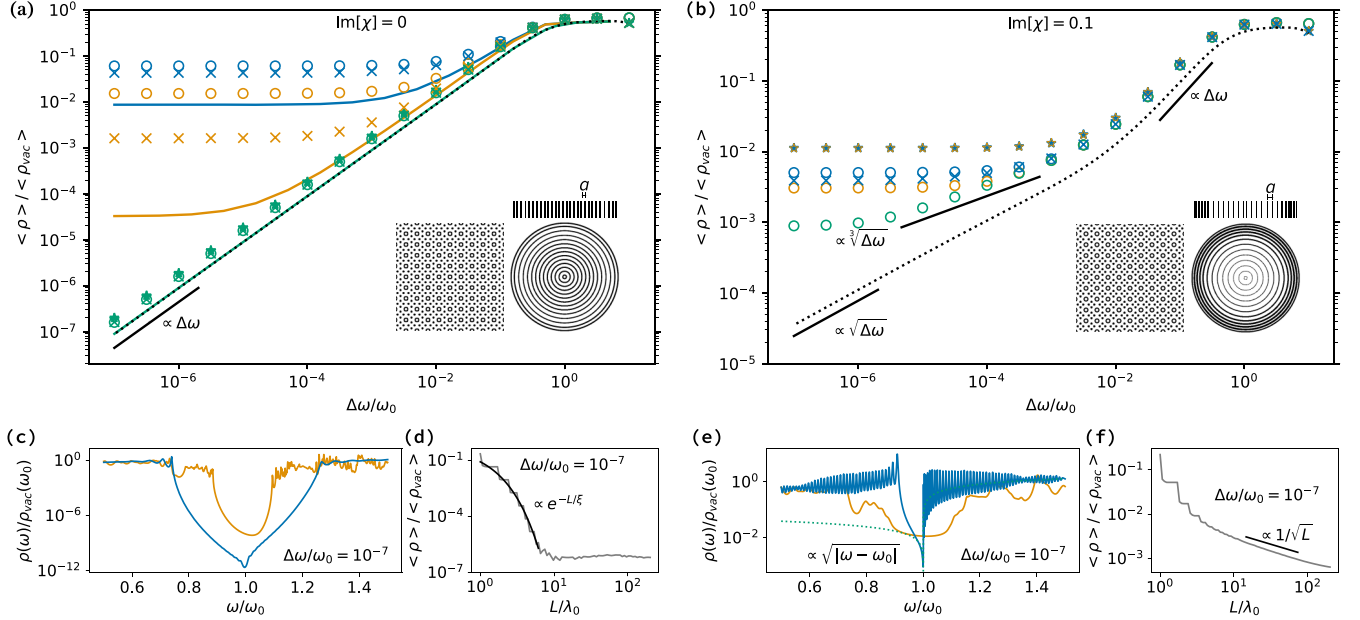


FIG. 2. (a) and (b) Lower bounds on bandwidth-integrated LDOS. All curves and markers refer to TM line sources located at the center of $L \times L$ design domains with (a) $\chi = 4$ for $L/\lambda_0 = \{1, 1.59, 10\}$ (blue, orange, green) and (b) $\chi = 4 + 0.1i$ for $L/\lambda_0 = \{5, 10, 80\}$ (blue, orange, green) where $\lambda_0 = 2\pi c/\omega_0$. Solid lines are lower bounds for finite $L \times L$ design domains, while dotted lines pertain to infinite systems, $L/\lambda_0 \rightarrow \infty$, computed via Eq. (11). All results are normalized by the corresponding bandwidth-integrated LDOS in vacuum. Markers correspond to structures discovered via topology optimization, where circles (\circ) are over rotationally symmetric structures, stars (\star) are for truncated 2Dd square-lattice photonic crystals of period λ_0 , and crosses (\times) allow for arbitrary structuring. Insets of (a) and (b): Representative inverse designs corresponding to $\Delta\omega/\omega_0 = 10^{-7}$ for a $10\lambda_0 \times 10\lambda_0$ design region. (c) and (e) Representative spectra for $L/\lambda_0 \gg 1$ [orange for $10\lambda_0 \times 10\lambda_0$ crystal, blue for $80\lambda_0 \times 80\lambda_0$ bullseye grating (not shown)]; optimizing over cylindrical geometries, the lossless and dispersionless case converges to a bullseye geometry of radial periodicity $a = \frac{\lambda_0}{4} \frac{1+\sqrt{1+\chi}}{\sqrt{1+\chi}}$ and ring thickness $h = \frac{\lambda_0}{4\sqrt{1+\chi}}$ (a radial quarter-wave stack) supporting a pseudogap centered around ω_0 [see (c)]; the lossy case converges to a radial chirped grating of initial spacing $a = \lambda_0/2$ and tapered thickness, causing the net absorbed power to come arbitrarily close to zero at ω_0 as $L \rightarrow \infty$, in the vicinity of which the system exhibits square-root dispersion [see (e)]. (d) and (f) The bandwidth-averaged LDOS of optimized bullseye structures within a design region of diameter L . The lossless (lossy) case demonstrates exponential (inverse square root) approach as a function of L to a positive saturation value due to a nonzero bandwidth $\Delta\omega/\omega_0 = 10^{-7}$.

requiring that $\text{Im}[\chi(\tilde{\omega})] > 0$ be positive [26]. While a complex susceptibility at real frequencies indicates material loss/gain [19], at complex frequencies dispersion and loss both contribute to $\text{Im}[\chi]$, with $\text{Im}[\chi(\tilde{\omega})] \rightarrow \text{Im}[\chi(\omega_0)]$ as $\Delta\omega \rightarrow 0$. Thus, $\text{Im}[\chi(\tilde{\omega})] = 0$ may be interpreted as a transparent and nondispersive medium.

Results. While below we focus on 2D TM sources, similar observations hold for either 2D transverse electric (TE) or 3D dipole sources, albeit with the electrostatic α term in those settings becoming relevant (and increasingly important at larger bandwidths). As detailed in Ref. [13] and the Supplemental Material (SM) [27], bounds on $\text{Im}[\frac{s(\tilde{\omega})}{\tilde{\omega}\mathcal{N}}]$ can be computed numerically for an arbitrary domain, here chosen as a square volume $V = L \times L$. For an infinite design space ($L \rightarrow \infty$), all operators and fields can be expanded in a spectral basis conforming to the symmetry of the domain—vector cylindrical waves [23,24]—yielding the following semianalytic expression for the bound,

$$\langle \rho_{\text{sca}} \rangle_{L \rightarrow \infty} \geq -\frac{1}{8\pi\mathcal{N}} \int_0^\infty dk k \left[\text{Im} \left(\frac{e^{i\theta}}{\chi^*} + \frac{e^{-i\theta}\tilde{\omega}^2}{k^2 - \tilde{\omega}^2} \right) \right]^{-1} \quad (10)$$

$$\times \text{Re} \left[\left| \frac{\tilde{\omega}}{k^2 - \tilde{\omega}^2} \right|^2 - \frac{e^{-i\theta}\tilde{\omega}^2}{(k^2 - \tilde{\omega}^2)^2} \right], \quad (11)$$

where maximization over the parameter θ can be computed numerically (see SM [27]). To lowest order in the bandwidth, for $\text{Im}[\chi] \geq 0$, this integral can be further simplified to yield the following asymptotic expression:

$$\frac{\langle \rho \rangle_{L \rightarrow \infty}}{\langle \rho_{\text{vac}} \rangle} \geq \sqrt{\frac{2\text{Im}[\chi]}{|\chi|^2}} \frac{\Delta\omega}{\omega_0} + O(\Delta\omega). \quad (12)$$

Thus, the bounds suggest near-perfect suppression is possible as $\Delta\omega \rightarrow 0$ even for $\text{Im}[\chi] > 0$ (consistent with zero material and radiative losses). Below, we present a physical mechanism that confirms this finding.

Figure 2 shows lower bounds on $\langle \rho \rangle$ obtained for finite $L \times L$ design regions along with achievable objective values discovered via inverse design. As the design footprint increases, inverse designs approach the limit given by the semianalytical result of Eq. (11), corresponding to $L \rightarrow \infty$. For $L/\lambda_0 = 10$, where $\lambda_0 = 2\pi c/\omega_0$ is the wavelength of the center frequency, the structures discovered via inverse design are within a factor of 2 of the infinite-space bounds for small $\text{Im}[\chi(\tilde{\omega})]$, but loosen by a couple of orders of magnitude for smaller ($L/\lambda_0 \lesssim 4$) device footprints (partly due to the associated bound relaxations). As seen, emission suppression for a TM source can be achieved through wave interference

generated by either Bragg grating arrangements of dielectric material or 2D PhCs, resulting in either pseudogaps or complete band gaps centered around ω_0 , respectively. For lossless materials, a 2D PhC of band-gap size ω_g centered at ω_0 has $\rho_{\text{phc}}(\omega) = 0$ for $|\omega - \omega_0| \leq \omega_g/2$, yielding an average $\langle \rho \rangle = \int_0^\infty \rho_{\text{phc}}(\omega) W(\omega) d\omega \propto \Delta\omega$ as $\Delta\omega \rightarrow 0$, consistent with the scaling of the bounds seen in Fig. 2(a).

In systems with material loss, $\text{Im}[\chi(\omega_0)] > 0$, one might expect LDOS to saturate to a small but positive value $\rho(\omega_0) > 0$ due to absorption by the structure. However, as confirmed in Fig. 2, the bounds of Eq. (12) suggest that complete emission cancellation is possible, with perfect suppression approached under vanishing bandwidth, $\Delta\omega \rightarrow 0$, albeit at a reduced $\sqrt{\Delta\omega}$ rate compared to the lossless case. Topology optimization discovers radial tapers (chirped gratings) with an initial spacing $a = \lambda_0/2$ but increasing thickness, producing an LDOS spectrum $\rho_{\text{taper}}(\omega) \approx \sqrt{|\omega - \omega_0|}$ [Fig. 2(b) inset] that meets at a nonzero plateau around ω_0 due to absorption in the medium. Such structures initially yield $\langle \rho \rangle = \int_0^\infty \rho_{\text{taper}}(\omega) W(\omega) d\omega \propto \sqrt{\Delta\omega}$ but absorption ultimately leads to nonzero saturation as $\Delta\omega \rightarrow 0$.

Since losses in the limit of vanishing bandwidth are ultimately dominated by absorption (as opposed to radiation), reducing the amount of material is crucial to LDOS minimization. However, material reduction is in conflict with the demands of nonzero bandwidth operation: In 2D PhCs, a minimum index contrast is required for the formation of a band gap [16,17], which implies a minimum fill fraction for any given index contrast (from perturbation theory). This is not an issue for effective 1D structures capable of supporting band gaps for any nonzero index contrast [16], which intuitively explains the performance advantage of bullseye gratings over 2D PhCs in Fig. 2. To further understand the engineering and performance of such quasi-1D designs, we exploit transfer matrices to study a 1D cavity design schema consisting of a central vacuum layer of thickness d (containing the source at the center) sandwiched by two identical half-infinite PhC claddings of susceptibility χ , unit cell size a , and material layer thickness h . The electric field within such a cavity, $|z| \leq d/2$, has the form $E(z; \omega) = E_0 e^{i\omega|z|} + E_0 r e^{i\omega d} e^{-i\omega|z|}$, where r is the reflection coefficient of the cladding, and the power output of the dipole is given by

$$\frac{\rho(\omega)}{\rho_{\text{vac}}(\omega)} = \frac{1 - |r|^2}{|1 - r e^{i\omega d}|^2}. \quad (13)$$

Perfect emission suppression can thus occur if $1 - |r|^2 \rightarrow 0$ and the denominator does not also approach zero.

One plausible strategy to achieve this condition is to design the PhC claddings such that ω_0 is at the band-gap center ω_m , and to take $h \rightarrow 0$. For lossless χ , first-order perturbation theory gives the size of the band gap ω_g as $\omega_g/\omega_m \approx \text{Re}[\chi]_a^h \propto h$ for $h/a \ll 1$ [16]. An oscillating dipolar source with frequency within the band gap will excite localized evanescent states with an exponential field decay constant $\gamma \propto \sqrt{\omega_g/\kappa}$ where κ is the band curvature at the band edge. This state does not radiate and without material loss, the LDOS is strictly zero. With loss, the absorbed power $P_{\text{abs}} = \int \text{Im}[\chi(z)] |E(z)|^2 dz \propto \text{Im}[\chi]_a^h \int e^{-2\gamma z} dz \propto h/\gamma$ (strictly speaking, material loss also

increases γ , so this proportionality is an upper bound). Since $\omega_g \propto h$, it may appear that $P_{\text{abs}} \propto h/\gamma \propto \sqrt{h}$ as $h \rightarrow 0$; however, the curvature at the band edge $\kappa \propto 1/h$ also depends on h so ultimately P_{abs} approaches a constant as $h \rightarrow 0$. In other words, exponential decay on its own is insufficient since the decay length diverges as the band gap closes, which limits the minimum absorption possible. Correspondingly, as $h \rightarrow 0$, the reflectivity at the midgap approaches

$$r(\omega_m) \approx \frac{i\chi}{\text{Im}[\chi] + \sqrt{(\chi + i\text{Im}[\chi]) \text{Re}[\chi]}}, \quad (14)$$

with $|r| < 1$ given $\text{Im}[\chi] > 0$, i.e., no perfect suppression.

A strategy that does produce near-perfect suppression is to engineer the cladding so ω_0 is not at the midgap but at the *upper band-gap edge*; this can be achieved by setting the unit cell size $a = \lambda_0/2$ and taking $h \rightarrow 0$. In this case

$$r(\omega_0) \approx -1 + \frac{\omega_0 h}{\sqrt{3}} - i\omega_0 h, \quad h \rightarrow 0, \quad (15)$$

independent of the material susceptibility, and we have $1 - |r|^2 \rightarrow 0$; to avoid division by zero in Eq. (13), one may choose $d \neq (n + \frac{1}{2})\lambda_0$ where n is a non-negative integer, in which case $\rho(\omega_0)/\rho_{\text{vac}}(\omega_0) \approx \frac{\pi}{\sqrt{3}} \sec^2(\frac{\omega_0 d}{2}) \frac{h}{\lambda_0}$ as $h \rightarrow 0$. Intuitively, in the limit of $h \rightarrow 0$, ω_0 approaches the band edge from above and the electric field profile approaches a standing wave (a slow light mode [28]) with field nodes inside material layers. Thus, by making the thicknesses of the PhC mirrors arbitrarily thin, one can ensure arbitrarily small field overlap with the lossy medium and thus vanishing absorption. This is reminiscent of techniques for linear optical control of light in coherent tunable absorbers [29–31], with the difference that the standing wave is not the result of interfering multiple incident waves but is a mode of the PhC itself.

The bandwidth-integrated LDOS for the 1D structure can also be computed and is given by $\frac{\langle \rho \rangle}{\langle \rho_{\text{vac}} \rangle} = \text{Re} \frac{1 + r e^{i\omega d}}{1 - r e^{i\omega d}} \frac{1}{\omega N}$. For $\Delta\omega \ll \omega_0$ and $d \not\approx (n + \frac{1}{2})\lambda_0$, we find that the optimal slow light cavity design has thickness $h = \lambda_0 \sqrt[3]{\frac{\Delta\omega}{\omega_0 \beta}}$, which yields

$$\frac{\langle \rho \rangle}{\langle \rho_{\text{vac}} \rangle} = \frac{\pi}{\cos^2(\frac{\omega_0 d}{2})} \text{Re} \left[\sqrt{\frac{1}{3} + \frac{i\beta\chi^*}{2\pi^2|\chi|^2}} \right] \sqrt[3]{\frac{\Delta\omega}{\omega_0 \beta}}, \quad (16)$$

where $\beta = \frac{2\pi^2 \text{Im}[\chi]}{3} [-1 + \sqrt{9 + 8(\frac{\text{Re}[\chi]}{\text{Im}[\chi]})^2}]$, proving the existence of structures exhibiting $\sqrt[3]{\Delta\omega}$ scaling, with

$$\frac{\langle \rho \rangle}{\langle \rho_{\text{vac}} \rangle} = \sqrt[3]{\frac{\pi}{2\sqrt{3}|\text{Re}[\chi]|} \frac{\Delta\omega}{\omega_0}} \left(1 + \frac{\sqrt{2}}{3} \frac{\text{Im}[\chi]}{|\text{Re}[\chi]|} + O(\text{Im}[\chi]^2) \right), \quad (17)$$

in agreement with inverse designs (before saturation due to finite device footprint) in Fig. 2. It remains an open question whether the bounds are loose or there exist structures with infinitely long tapering that may indeed achieve the faster $\sqrt{\Delta\omega}$ scaling of Eq. (11).

The proposed strategy for absorption cancellation is only useful in situations where extinction is dominated by absorption. In particular, achieving near-perfect suppression also relies on an infinite device size where radiative losses can be

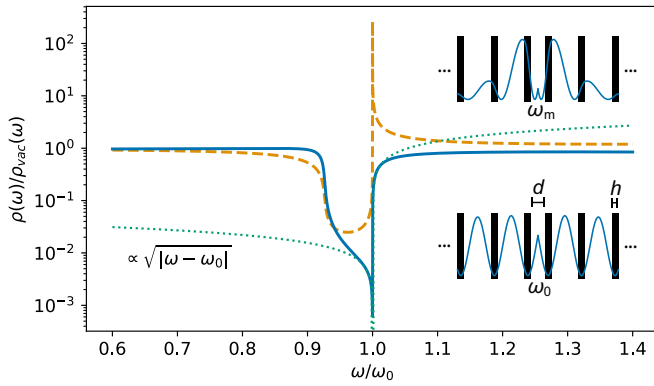


FIG. 3. LDOS spectrum, Eq. (13), of a 1D PhC cavity with period $a = \lambda_0/2$, material layers of thickness $h = a/50$, and a central air gap of thickness $d = \{a/3, a - h\}$ (solid blue, dashed orange, respectively) with loss $\text{Im}[\chi(\omega)] = 0.1$. The dotted green curve shows a square-root fit around ω_0 . The inset is a representative intensity profile $|E(z; \omega_0)|^2$ at the band edge, exhibiting minima in the material layers (vertical black bars), as well as $|E(z; \omega_m)|^2$ at the pseudomidgap, exhibiting minima adjacent to the material layers for $d = a/3$.

eliminated: As seen in Fig. 2, $\rho(\omega_0) \rightarrow 0$ only as $L \rightarrow \infty$. In the lossless case, $\rho(\omega_0) \propto \exp(-L/\xi)$ for some length scale ξ consistent with exponential localization [32–34]. In the lossy case, inverse design converges on adiabatic tapers consisting of rings of vanishing thickness in the vicinity of the emitter, leading to $\rho(\omega_0) \propto 1/\sqrt{L}$, with tapering appearing to reduce reflections from the finite interface.

Finally, note that $d \approx (n + \frac{1}{2})\lambda_0$ can be understood as an off-resonance condition for the cavity formed by these slow light mirrors: If d is chosen to be on resonance, then instead of suppression the system produces enhancement. Specifically, setting $d = a - h \approx \frac{\lambda_0}{2}$ forms a complete PhC and leads to $\rho(\omega_0)/\rho_{\text{vac}}(\omega_0) \approx \frac{\sqrt{3}}{\pi} (\frac{h}{\lambda_0})^{-1}$ as $h \rightarrow 0$, enhancing LDOS near ω_0 (Fig. 3, dashed orange curve). For a fixed material layer thickness h , such structures initially yield $1/\sqrt{\Delta\omega}$ divergence in $\langle \rho \rangle$ but absorption ultimately leads to finite saturation as

$\Delta\omega \rightarrow 0$. Optimizing the material thickness at each $\Delta\omega$ produces an analogous diverging integrated LDOS enhancement $\frac{\langle \rho \rangle}{\langle \rho_{\text{vac}} \rangle} \propto 1/\sqrt[3]{\Delta\omega}$ as $\Delta\omega \rightarrow 0$. This confirms the previously unexplained prediction in Ref. [13] that diverging extinction power is possible in the presence of loss without having to come arbitrarily close to field singularities at infinitely sharp tips [19,35–38]. (Note that Ref. [13] finds a weaker $1/\sqrt[4]{\Delta\omega}$ bandwidth dependence as the emitter is adjacent to rather than surrounded by the structured medium.) In practice, achievable extinction powers will ultimately rest on fabrication and material tolerances. Fortunately, the predicted cube root scaling of the optimal material thickness on the bandwidth suggests fabricable feature sizes for moderate bandwidths: considering $\Delta\omega/\omega_0 = 10^{-3}$ and silicon, with $\chi = 11.8 + 3.6 \times 10^{-3}i$ at near-infrared $\lambda_0 = 1 \mu\text{m}$ wavelengths, the optimal thickness $h \approx 15 \text{ nm}$, within reach of electron-beam lithography. Lastly, we remark once more that while we focused here on TM fields (applicable to thin-film slab geometries), similar conclusions follow for 2D TE and 3D fields. Likewise, while we focused on dielectrics, the formalism is applicable to metals as well.

Acknowledgments. This work was supported by the Cornell Center for Materials Research (MRSEC) through Award DMR-1719875. R.K.D. gratefully acknowledges financial support from the Princeton Presidential Postdoctoral Research Fellowship and from the National Academies of Science, Engineering, and Medicine Ford Foundation Postdoctoral Fellowship program. S.M. acknowledges financial support from the Canada First Research Excellence Fund via the Institut de Valorisation des Données (IVADO) collaboration. The simulations presented in this article were performed on computational resources managed and supported by Princeton Research Computing, a consortium of groups including the Princeton Institute for Computational Science and Engineering (PICSciE) and the Office of Information Technology’s High Performance Computing Center and Visualization Laboratory at Princeton University. The views, opinions, and findings expressed herein are those of the authors and should not be interpreted as representing the official views or policies of any institution.

- [1] E. M. Purcell, On the absorption and emission of light by interstellar grains, *Astrophys. J.* **158**, 433 (1969).
- [2] G. Colas des Francs, P. Bramant, J. Grandier, A. Bouhelier, J.-C. Weeber, and A. Dereux, Optical gain, spontaneous and stimulated emission of surface plasmon polaritons in confined plasmonic waveguide, *Opt. Express* **18**, 16327 (2010).
- [3] J. Michon, M. Benzaouia, W. Yao, O. D. Miller, and S. G. Johnson, Limits to surface-enhanced Raman scattering near arbitrary-shape scatterers, *Opt. Express* **27**, 35189 (2019).
- [4] S. V. Gaponenko, D. V. Guzатов, and N. D. Strekal, Strong selective anti-Stokes Raman scattering enhancement in plasmonics using photon density of states engineering, *J. Phys. Chem. C* **125**, 27654 (2021).
- [5] P. Wang and R. Menon, Optimization of generalized dielectric nanostructures for enhanced light trapping in thin-film photovoltaics via boosting the local density of optical states, *Opt. Express* **22**, A99 (2014).
- [6] J. C. Cuevas and F. J. García-Vidal, Radiative heat transfer, *ACS Photon.* **5**, 3896 (2018).
- [7] Z. Lin, X. Liang, M. Lončar, S. G. Johnson, and A. W. Rodriguez, Cavity-enhanced second-harmonic generation via nonlinear-overlap optimization, *Optica* **3**, 233 (2016).
- [8] E. M. Purcell, Spontaneous emission probabilities at radio frequencies, in *Confined Electrons and Photons: New Physics and Applications* (Springer, Berlin, 1995), p. 839.
- [9] E. Yablonoitch, Inhibited spontaneous emission in solid-state physics and electronics, *Phys. Rev. Lett.* **58**, 2059 (1987).
- [10] S. Molesky, P. Chao, W. Jin, and A. W. Rodriguez, Global T operator bounds on electromagnetic scattering: Upper bounds on far-field cross sections, *Phys. Rev. Res.* **2**, 033172 (2020).
- [11] H. Shim, L. Fan, S. G. Johnson, and O. D. Miller, Fundamental limits to near-field optical response over any bandwidth, *Phys. Rev. X* **9**, 011043 (2019).

- [12] P. Chao, B. Strekha, R. K. Defo, S. Molesky, and A. W. Rodriguez, Physical limits in electromagnetism, *Nat. Rev. Phys.* **4**, 543 (2022).
- [13] P. Chao, R. K. Defo, S. Molesky, and A. Rodriguez, Maximum electromagnetic local density of states via material structuring, *Nanophotonics* **12**, 549 (2023).
- [14] X. Liang and S. G. Johnson, Formulation for scalable optimization of microcavities via the frequency-averaged local density of states, *Opt. Express* **21**, 30812 (2013).
- [15] E. Yablonovitch, Photonic crystals, *J. Mod. Opt.* **41**, 173 (1994).
- [16] J. D. Joannopoulos, S. G. Johnson, J. N. Winn, and R. D. Meade, *Photonic Crystals: Molding the Flow of Light*, 2nd ed. (Princeton University Press, Princeton, NJ, 2008).
- [17] M. C. Rechtsman and S. Torquato, Method for obtaining upper bounds on photonic band gaps, *Phys. Rev. B* **80**, 155126 (2009).
- [18] K. M. Ho, C. T. Chan, C. M. Soukoulis, R. Biswas, and M. Sigalas, Photonic band gaps in three dimensions: New layer-by-layer periodic structures, *Solid State Commun.* **89**, 413 (1994).
- [19] L. Novotny and B. Hecht, *Principles of Nano-Optics*, 2nd ed. (Cambridge University Press, Cambridge, U.K., 2012).
- [20] K. Joulain, R. Carminati, J.-P. Mulet, and J.-J. Greffet, Definition and measurement of the local density of electromagnetic states close to an interface, *Phys. Rev. B* **68**, 245405 (2003).
- [21] W. R. Hindmarsh and D. ter Haar, *Atomic Spectra: The Commonwealth and International Library: Selected Readings in Physics* (Elsevier Science, Amsterdam, 2014).
- [22] L. D. Landau, E. M. Lifšic, L. P. Pitaevskii, and L. D. Landau, *Electrodynamics of Continuous Media*, Course of Theoretical Physics, 2nd ed. (Elsevier/Butterworth-Heinemann, Amsterdam/Heidelberg, 2009), Vol. 8.
- [23] W. C. Chew, *Waves and Fields in Inhomogeneous Media* (Wiley, New York, 1999), Vol. 16.
- [24] L. Tsang, J. A. Kong, and K.-H. Ding, *Scattering of Electromagnetic Waves: Theories and Applications* (Wiley, New York, 2004), Vol. 27.
- [25] J. D. Jackson, *Classical Electrodynamics*, 3rd ed. (Wiley, New York, 1999).
- [26] H. Hashemi, C.-W. Qiu, A. P. McCauley, J. D. Joannopoulos, and S. G. Johnson, Diameter-bandwidth product limitation of isolated-object cloaking, *Phys. Rev. A* **86**, 013804 (2012).
- [27] See Supplemental Material at <http://link.aps.org/supplemental/10.1103/PhysRevA.109.L041501> for further details on the derivations of the presented semianalytic expressions, asymptotics, and numerical results.
- [28] T. Baba, Slow light in photonic crystals, *Nat. Photon.* **2**, 465 (2008).
- [29] J. Zhang, K. F. MacDonald, and N. I. Zheludev, Controlling light-with-light without nonlinearity, *Light: Sci. Appl.* **1**, e18 (2012).
- [30] N. Gutman, A. A. Sukhorukov, Y. D. Chong, and C. M. de Sterke, Coherent perfect absorption and reflection in slow-light waveguides, *Opt. Lett.* **38**, 4970 (2013).
- [31] D. G. Baranov, A. Krasnok, T. Shegai, A. Alù, and Y. Chong, Coherent perfect absorbers: Linear control of light with light, *Nat. Rev. Mater.* **2**, 17064 (2017).
- [32] M. D. Leistikow, A. P. Mosk, E. Yeganegi, S. R. Huisman, A. Lagendijk, and W. L. Vos, Inhibited spontaneous emission of quantum dots observed in a 3D photonic band gap, *Phys. Rev. Lett.* **107**, 193903 (2011).
- [33] A. A. Asatryan, K. Busch, R. C. McPhedran, L. C. Botten, C. M. de Sterke, and N. A. Nicorovici, Two-dimensional Green's function and local density of states in photonic crystals consisting of a finite number of cylinders of infinite length, *Phys. Rev. E* **63**, 046612 (2001).
- [34] E. Yeganegi, A. Lagendijk, A. P. Mosk, and W. L. Vos, Local density of optical states in the band gap of a finite one-dimensional photonic crystal, *Phys. Rev. B* **89**, 045123 (2014).
- [35] M. Idemen, Confluent tip singularity of the electromagnetic field at the apex of a material cone, *Wave Motion* **38**, 251 (2003).
- [36] B. V. Budaev and D. B. Bogy, On the electromagnetic field singularities near the vertex of a dielectric wedge, *Radio Sci.* **42**, RS6S08 (2007).
- [37] P. J. Schuck, D. P. Fromm, A. Sundaramurthy, G. S. Kino, and W. E. Moerner, Improving the mismatch between light and nanoscale objects with gold bowtie nanoantennas, *Phys. Rev. Lett.* **94**, 017402 (2005).
- [38] A. Kinkhabwala, Z. Yu, S. Fan, Y. Avlasevich, K. Müllen, and W. E. Moerner, Large single-molecule fluorescence enhancements produced by a bowtie nanoantenna, *Nat. Photon.* **3**, 654 (2009).